Spatiotemporal Drought Assessment Using Geospatial Artificial Intelligence and Satellite Imagery (Geoai-Eo) Techniques in Arid Land

Dr.. Ayoub Ahmed Abdullah Almhab
Consultant, Ministry of Agriculture, s and water resources, Sana'a, Yemen
Department of Agricultural Sciences (part time), Amran University, Amran, Yemen
Email: ayoub.almhab@gmail.com

Abstract

Drought is a major global climate change that causes decreased precipitation and increased temperatures and evaporation, leading to water shortages, agricultural decline, and population migration. Yemen's territory is located within arid and semi-arid regions, and is characterized by its diverse terrain, including coastal, mountainous, eastern plateau, and desert areas. Therefore, research studying the phenomenon of drought is of great importance. In this study, drought was evaluated through a set of indicators, such as the Vegetation Condition Index, Normalize difference vegetation Index (NDVI) and the Drought Severity Index, to evaluate drought in the Yemeni regions. Using geospatial artificial intelligence and satellite imagery (GeoAI-EO) techniques to more accurately assess spatiotemporal drought, using a wide range of data. Dry months are found to last from October to April, while September is the least frequent month in the mountainous western regions. It was also found that drought is more common in the coastal areas and the eastern plateau than in the mountainous highlands and western slopes. Maps and graphs showed the difference in dry and wet climatic ranges of the drought coefficient and showed the extent of variation between regions and seasons.

Keywords: climate, drought, dry areas, drought coefficients, GeoAI-EO, Yemen.

1.   Introduction

Drought is one of the most important climate changes affecting the world, as it causes decreased rainfall rates, increased temperatures, and increased evaporation, leading to water shortages, a decline in agricultural production, and population migration. Drought can be evaluated through a set of indicators, such as the soil moisture index, the moisture fluctuation index, and the hydrological drought index. However, these traditional indicators rely on historical climate data, which may not be accurate in assessing spatiotemporal drought, especially in areas that suffer from the unavailability of climate stations and irregular climate data in addition to the fluctuations occurring with climate change. Artificial intelligence techniques can be used to more accurately assess spatiotemporal drought such as (Vegetation Condition Index, Normalize difference vegetation Index (NDVI) and the Drought Severity Index), as these techniques can use a wide range of data, including climate data, geographic data, and space data. The use of geospatial artificial intelligence and space imaging in Earth observation and spatiotemporal drought assessment has been done by many previous and current studies. Precipitation estimation from remote sensing information has been developed using artificial neural networks (PERSIANN), (Sorooshian et al., 2000). (Hsu et al., 1997))) at the Center for Hydrometry and Remote Sensing (CHRS) at the University of California, Irvine uses neural network technology to map the complex nonlinear functions involved in transferring remote sensing data to a form that can be used in Applications. While (Sharma et al., 2006) used spatial data mining techniques to extract drought patterns using Difference Vegetation Index (NDVI) and rainfall data. Both (Afzali et al., 2016) and (Ali et al., 2011) evaluated geostatistical methods for the spatial analysis of drought indicators, with Afzali focusing on the Zayandhrud River Basin in Iran and Ali in Bushehr Province. Ramkar and Yadav (2018) focused on the Tapi River Basin in India, using the rainfall index, standardized rainfall index, and reconnaissance drought index for temporal analysis, and the inverse distance measure method for spatial mapping. Shahabfar and Eitzinger (2013) evaluated six meteorological

drought indices in Iran, and identified Z-Score, China-Z Index, and Modified China-Z Index as effective predictors. (Khellouk et al., 2020) monitored surface soil moisture in a semi-arid region using Landsat-8 OLI images and developed a new model to estimate soil moisture content. Gebrehiwot (et al., 2011) assessed drought in the northern highlands of Ethiopia, using the standardized rainfall index and vegetation condition index to quantify spatial and temporal variation. (Houmma et al., 2022) provided a comprehensive overview of the latest developments in big data technologies for agricultural drought modeling, highlighting the use of multi-sensor remote sensing techniques and artificial intelligence. (Kikon and Deka, 2021) focus on applying artificial intelligence techniques in drought assessment, monitoring and forecasting, which underscores the need for a drought management system. Nohegar et al., 2013 also used geostatistical methods, especially kriging, to extract maps of drought indicators in southern Iran, and found that these methods were the most effective. (Hoque et al., 2021) and (Hoque et al., 2020) extended this approach to assess drought vulnerability in southern Queensland, Australia, and the northwestern region of Bangladesh, respectively. Both studies used a multi-criteria approach, combining meteorological, hydrological, agricultural and socio-economic factors to create comprehensive drought vulnerability maps. (Jain et al., 2015) also presented the Integrated Drought Vulnerability Index (IDVI) to assess spatial and temporal vulnerability, while (Afzali et al., 2016) evaluates different interpolation methods for mapping drought indices.

Agricultural drought in the Tihama Plain in Yemen was also assessed using the Standardized Precipitation Index (SPI) and Geographic Information Systems (GIS) (Hashim et al., 2017). This study concluded that the years 1984, 1991, 2002, 2003, 2004, 2005, 2006, and 2008 were the Highly affected by drought. A remote sensing-based assessment of water resources in the Arabian Peninsula, including Yemen, revealed declining rainfall trends and TWS anomalies (Wehbe and Temimi., 2021). Spatiotemporal analysis of drought in the Haihe River Basin in China, using the Standardized Evapotranspiration Index (SPEI), showed an increasing trend in drought frequency and severity (Yang et al., 2016). Similarly, an assessment of meteorological drought in West Azerbaijan Province, Iran, using the Standardized Precipitation Index (SPI), indicated an increase in drought duration with an increase in the return period and time scale (Nosrati and Zareiee 2011). Collectively, these studies highlight that spatial techniques have been effectively used in assessing drought severity and vulnerability in different regions of the world, the importance of the potential of Geo-artificial intelligence techniques and satellite imagery in enhancing the accuracy and effectiveness of spatiotemporal drought assessment, and the importance of considering indicators and parameters. Multiple studies in estimating drought, the potential of indicators based on remote sensing in arid regions, as well as the increasing severity and frequency of drought in Yemen and the need for further research and actions to address this problem. These results suggest that the most appropriate geostatistical method for the spatial analysis of SPI and EDI drought indices may vary depending on the specific location and indicator under study.

1.2 Research problem:

The problem of the research is that the phenomenon of drought is one of the frequently occurring climatic phenomena, and the location of its occurrence varies from one region to another, and from time to time in terms of severity and impact. It may continue for many years, and may cause economic and natural damage whose effects are reflected on humans and the environment. If the duration of the drought is short and severe, it is capable of causing huge losses to the local economy, and drought disasters may outweigh other natural disasters, including floods, in terms of negative effects. Therefore, recent studies have focused on studying drought and its serious effects on the environment in general, after the threat of drought began to

become more severe than it was previously, and what climate change factors have contributed to, in terms of the increasing frequency of drought periods and their increasing severity in recent times. Therefore, this study will attempt to answer the following questions:

How can drought trends in Yemen be determined?

How is drought distributed temporally and spatially over selected areas of Yemen?

What are the areas most affected by drought in Yemen?

1.3 The objectives:

It is a study of changes in the temporal and spatial extent of areas suffering from drought conditions across Yemen, using satellite data and geographical artificial intelligence GeoAI-EO. More specifically, the research aims to achieve the following objectives: Develop an artificial intelligence model for spatiotemporal drought assessment. Applying the model to drought data in Yemen. Evaluating the model's performance in spatiotemporally assessing drought.

1.4 Research Importance:

The development of drought is a slow and complex process that can be described using multiple indicators and variables. Documenting changes in drought conditions requires long-term records of observations with appropriate temporal and spatial coverage, and traditional methods for estimating drought indicators based on climate data from monitoring stations give data about the point where the monitoring station is located, in contrast to indicators derived from satellite images and combined with GeoAI-EO will cover large areas and provide data of utmost importance, especially in areas such as Yemen, where monitoring stations only cover a limited area of the country.

1.4 The most important terms

✓ **Artificial Intelligence (AI):** Artificial Intelligence is a field of computer science that focuses on developing computers that can think and act like humans.

✓ **Geospatial artificial intelligence** (GeoAI) is the field of artificial intelligence (AI) that uses geographic information systems (GIS) to analyze and interpret spatial data. Artificial intelligence that uses satellite Earth observations (EOs), which we call AI-EO. For the purpose of this research, we use the term (GeoAI-EO), which combines the two terms (geospatial artificial intelligence and space imaging.(

✓ **Definition and description of drought**: The development of drought conditions is a very slow and complex process. Therefore, the causes and mechanisms involved are still not fully understood. Factors contributing to the development of drought include rainfall, evaporation and soil conditions. All of these factors, in turn, are affected by climate, winds, and long-term atmospheric and oceanic fluctuations. There are multiple types of dehydration, although no formal definition has been agreed upon, the following types are generally accepted.

(Wilhite and Glantz, 1985) in (Fleig et al., 2006)

✓ **Metrological drought** = deficit in rainfall

✓ **Agricultural drought** = lack of soil moisture, which affects plant cover and food production. It also increases the risk of forest fires as plants are drier and more susceptible to fire.

✓ **Hydrological drought** = lack of surface water and/or groundwater.

Reduced drinking water supplies, hydroelectric potential and water for industrial needs affect wildlife and humans alike.

✓ **Socioeconomic drought** = measuring the impact of drought, including supply and demand. It is usually expressed as economic value. (Wilhite and Glantz, 1985) in (Fleig et al., 2006) and (Damberg, 2014).

2. **Materials and method**

This research relies on a range of methods and techniques, including: analysis of climate data, geographic data and space data. Developing artificial intelligence models. Evaluating the performance of artificial intelligence models. The descriptive analytical approach was used by reviewing a variety of sources, research, studies, books, technical reports, and experiences obtained about the role of GeoAI-EO in developing the agricultural sector, in addition to the analytical approach, a case study through data analysis of satellite images using various models based on To use the JavaScript language in the Google Earth Engine environment.

2.1 Study area
Yemen is located in the southwestern part of the continent of Asia and in the south of the Arabian Peninsula, between latitudes 12 degrees and 20 degrees north and longitudes 41 degrees and 54 degrees east. It is bordered to the north by the Kingdom of Saudi Arabia, to the east by Oman, to the south by the Arabian Sea and the Gulf of Aden, and to the west by the Red Sea, as shown in Figure (3.(
Yemen has a mostly semi-arid to arid climate. Rainy seasons occur during the spring and summer. Yemen's climate is strongly influenced by the mountainous nature of the country (Bruggeman, 1997). The rainfall rate rises from less than 50 mm in the coasts along the Red Sea and the Gulf of Aden. In the western highlands, water levels reach a maximum of 500-800 mm and decline steadily to less than 50 mm inland.

Figure 1 Location of the study area, Yemen

2.2 Indicators drought index
Table 1 below present the mean Collection of drought index, abbreviations and input parameters used in their computation.

Table 1 Collection of drought index, abbreviations and input parameters used in their computation

Abbreviation	Full name	Input parameters
SPI	Standardized Precipitation Index	Precipitation
PDSI	Palmer Severity Drought Index	Precipitation and temperature (longer timescale, meteorological drought)
Palmers Z-index	Palmer Z-index	Precipitation and temperature (shorter timescale)

PHDI	Palmer Hydrological Drought Index	Precipitation and temperature (longer timescale, hydrological drought)
SPEI	Standardized Precipitation Evaporation Index	Precipitation and Temperature
SWEI	Surface Water Supply Index	Precipitation, Reservoir storage, Snowpack and Streamflow
SRI	Standardized Runoff Index	Streamflow
VCI	Vegetation Cover Index	Remote Sensing Data
vegDRI	Vegetation Drought Response Index	Remote Sensing Data
NDVI	Normalized Difference Vegetation Index	Remote Sensing Data
NDWI	Normalized Difference Water Index	Remote Sensing Data
SMI	Soil Moisture Index	Soil Moisture Content, Wilting Point and Field Capacity
DR	Dependable Rain	Precipitation
NRI	National Rain Index (Africa)	Precipitation

Sources: (Damberg, 2014)

2

2.3 Standard precipitation index

The Standardized Precipitation Index (SPI) is one of the most widely used and recommended drought indicators (WMO, 2009: WCRP, 2010). The SPI ranges from -4 to +4 with negative and positive values indicating drought and wet periods, respectively. Figure 2 presents the concept of the SPI indicator. Since the index has maximum values of -4 for abnormally dry events and +4 for abnormally wet events, it can be interpreted It is defined as the number of standard deviations away from the mean for a given event (Edwards, 1997). According to SPI (McKee et al., 1993), values between -1 and -2 indicate moderate to severe droughts while an index of less than -2 indicates severe droughts.

Standard Normal Distribution

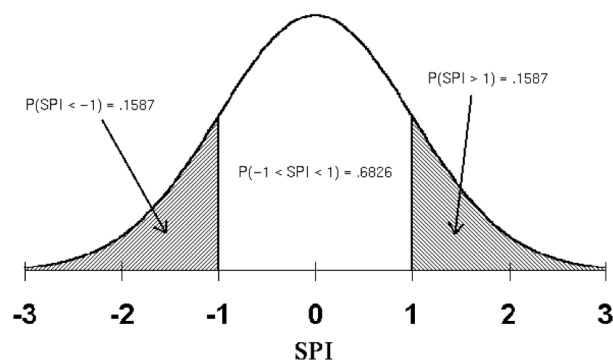P(SPI < −1) = .1587
P(−1 < SPI < 1) = .6826
P(SPI > 1) = .1587

SPI

Figure 2 Standard normal distribution with SPI with mean = and variance 1. The area below 1 represents areas experiencing moderate to severe drought conditions for future studies (Edwards, 1997(

2.4 Indicators from remote sensing data

The increase in remote sensing data has provided researchers with the opportunity to develop new types of indicators that rely directly on remote sensing data. Indicators that look at vegetation provide information about how vegetation responds

to water shortages, using high-resolution radiometer data (visible and near-infrared reflectance from surface instruments to satellites). This technology has been developed since the beginning of the seventies, when satellite monitoring began.

The positive aspects of the Native Vegetation Index (VCI) are its spatial resolution properties and how the data can be adjusted to suit climate, environment and weather. The disadvantages are that VCI is mainly useful during the summer season as large areas are covered with dormant plants during the winter seasons. This represents a particular problem for the indicator in temperate climate regions with strong seasons (Mishra and Singh, 2010).

Other indices based on remote sensing data, the Normalized Difference Water Index (NDWI) and the Normalized Difference Vegetation Index (NDVI), are also useful for assessing drought. NDVI records have been available globally since 1981 at 8 km resolution. The NDVI index uses the difference between near red and visible infrared reflectance to indicate changes in chlorophyll and intercellular space in plants. High NDVI values reflect healthy vegetation while low values show pressure on vegetation for the same time frame. Both drying and humidification can be shown in the NDVI index. In the development of the NDWI, the same satellite products are used with shortwave infrared data making it possible to retrieve changes in water content in vegetation (Gu et al., 2008). However, according to Gu et al. (2008). The Soil Moisture Deficit Index (SMDI) and the Evapotranspiration Deficit Index (EDI), both developed by (Narasimhand and Srinivan in 2005), are based on simulated outputs from hydrological models calibrated on a weekly scale. In 2009, a soil moisture index (SMI) was proposed which included wilting point and field capacity (Mishra and Singh, 2010). For Africa, there is an index called Dependable Rains, based on statistical rainfall occurring four out of five years in 1993 and a year later it was converted to the National Rainfall Index (RI). RI was calculated from rain gauges at the national level and was mainly used to characterize patterns at the local level. Another regional attempt to monitor droughts is the Australian Drought Monitoring System, which is based on consecutive months in which rainfall is below the threshold (Heim, 2002). In the United States, the drought monitor includes multiple indicators and monitoring groups (Svoboda et al., 2002).

2.6 Remote sensing data

Obtaining long-term rainfall data is essential for reliable drought analysis. With the advent of satellite records and the improvement of their results, there is a new possibility for model independent data to emerge, which can be used to validate and verify models (AghaKouchak et al., 2012). Since the turn of the millennium, several satellite-based products have provided the most accurate real-time and accurate global precipitation estimates (e.g., the Tropical Rainfall Measurement Mission (TRMM) and Multisatellite Precipitation Analysis (TMPA)) (Huffman et al., 2007). One limitation of real-time satellite-derived rainfall estimates is the short The data is relatively long (currently 10-13 years).One long-term estimate of precipitation Which dates back to 1979, but with a real-time lag, is the revised measure of the Global Precipitation Climatology Project. Although significant effort has been made to statistically validate satellite products, improvements are still needed in various areas, for example in pattern recognition (AghaKouchak et al., 2011) and in bias correction algorithms,   Behrangi et al. (2011). According to (AghaKouchak et al., 2012) the lack of information regarding reliability and uncertainties in most products is real-time, and it has not been integrated into the application outside the research community yet. Below is a presentation of the rainfall datasets used in the study as well as an overview of the combination of multiple modes used.

2.7 Estimating rainfall from remote sensing information using artificial neural networks (PERSIANN)

Precipitation estimation from remote sensing information using artificial neural networks (PERSIANN, (Sorooshian et al., 2000); (Hsu et al., 1997)) was developed at the Center for Hydrometry and Remote Sensing (CHRS) at the University of California , Irvine and uses neural network technology to map the complex nonlinear functions involved in transferring remote sensing data into a form that can be used in applications. How the process works is shown in the diagrams in Figure 3, where the first layer is the input layer, then there is a hidden layer and finally the output layer. Layers are connected by weighted links between nodes of different layers. The hidden layer values depend on the input values and those links are weighted and the output values are linked to the hidden layer accordingly. While training a neural network, an optimization dataset is used, where the input and output values are known, and optimization algorithms that minimize the difference between observed and desired outputs provide information about weighted connections. In (Sorooshian et al., 2000) a detailed explanation of how algorithms are used to produce the estimation product, which is a raster map with a 0.5 × 0.5 degree grid provided daily, 3- and 6-hourly precipitation on a global scale. . The PERSIANN system was based on geostationary infrared images (later extended to include the use of both visible infrared and daytime visible images (Center for Hydrometeorology and Remote Sensing, 2004.(
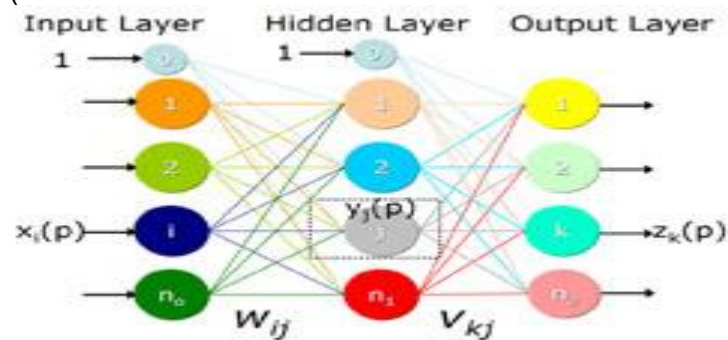

Figure 3 Process diagrams in the ANN learning algorithm, where the lines between the nodes are weighted links whose weights are determined by the optimization algorithms (Center for Hydrometeorology and Remote Sensing, 2004.(

2.7 Google Earth Engine
In the world of geospatial AI, the Google Earth Engine is emerging as a powerful force. It provides a cloud platform to harness the huge archive of satellite images. This treasure enables researchers and environmental experts to delve deeper into understanding our planet. One crucial application is in monitoring and measuring drought. Using GEE, users can access datasets such as temperature fluctuations, precipitation patterns, and vegetation health derived from satellite observations. These rich layers of data then pave the way for calculating various drought parameters – indicators that determine the severity and spread of drought episodes. From standardized precipitation indices to vegetation condition indices, GEE facilitates their calculation over large areas and provides detailed insights into drought dynamics. This capacity proves invaluable for resource management, agricultural planning, and early warning systems, ultimately helping communities prepare for and mitigate the impacts of these challenging environmental events.
Google Earth enables us to extract valuable information about droughts from its huge satellite data archive. We start by defining our region and time frame, then choose relevant datasets such as Landsat or Sentinel-2 images and robust drought indices such as NDVI or SPEI. Filtering out unwanted items and performing time series analysis allows us to extract key insights. Finally, thematic maps and data integration tell the story of drought severity and its relationship to factors such as soil moisture.

This enables informed decisions and mitigation strategies. To explore further, see the Google Earth Engine tutorials and community forums (https://earthengine.google.com./).

3.   Preliminary Results and Indicators
3.1 Introduction
The results were presented based on the preliminary results of the spatial drought indicators for various regions of Yemen and southwestern Arabia, as well as the preliminary results of the time series indicators of drought for different regions of Yemen according to the available periods. The period in the figure was reduced to several years so that the figure appears clearly. We tried Increase the time period in the general average for Yemen so that it is as clear as possible.

3.2 Preliminary Results of Spatial Drought Indicators
The maps, created using JavaScript code in Google Earth, show that drought varies greatly across Yemen(https://code.earthengine.google.com/29938f5fcf023a281d71f98323cb0281).
3.2.1 Vegetation condition Index (VCI)
The Vegetation Condition Index (VCI) figure 4 map of Yemen shows that large areas of the country are suffering from severe drought. In 2023, the average VCI in Yemen was about 0.6, indicating that vegetation in Yemen had declined by up to 40%.
The vegetation condition factor classification map shows that most areas of Yemen fall into the "severe drought" or "exceptional drought" category. Only small areas in the extreme north and south of the country fall into the "normal" or "humid" category.
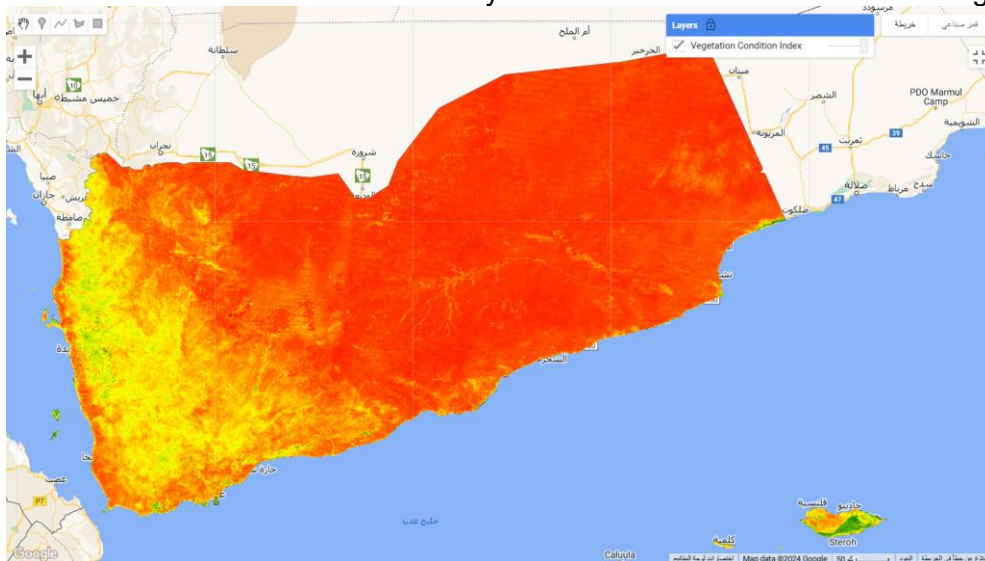

Figure 4 shows a map of the Vegetation Condition Index in Yemen
3.2.2 The Drought Severity Index (DSI)
The Drought Severity Index (DSI) figure 5 classification map shows that drought is particularly affecting the West Coast and Tihama Plain regions. In 2023, the average DSI in these areas was about 0.8, indicating that the drought is very severe. And Figure 6 show the Vegetation Condition Index classification map in Yemen.
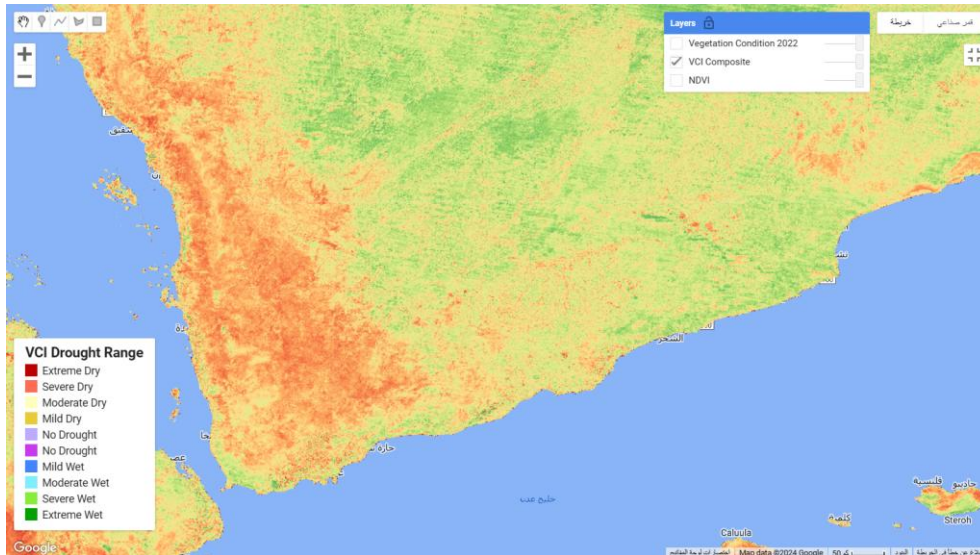
Figure 5 shows the Vegetation Condition Index classification map in Yemen
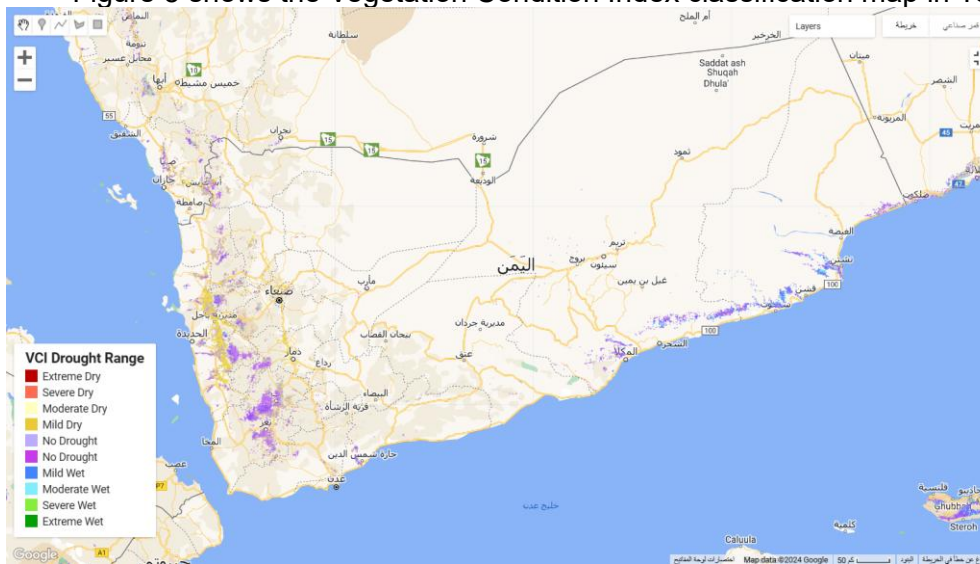

Figure 6 shows the Vegetation Condition Index classification map in Yemen (places that do not suffer from drought)

3.2.3 Normalize difference vegetation Index (NDVI)

The NDVI map Figure 7 shows that drought has greatly affected vegetation in Yemen. In 2023, the average NDVI in Yemen would be around 0.3, indicating an up to 70% reduction in vegetation compared to 2000. And figure 8 shows the Drought Severity Index classification map in Yemen, and Figure 9 shows the Vegetation Condition Index classification map in Yemen.
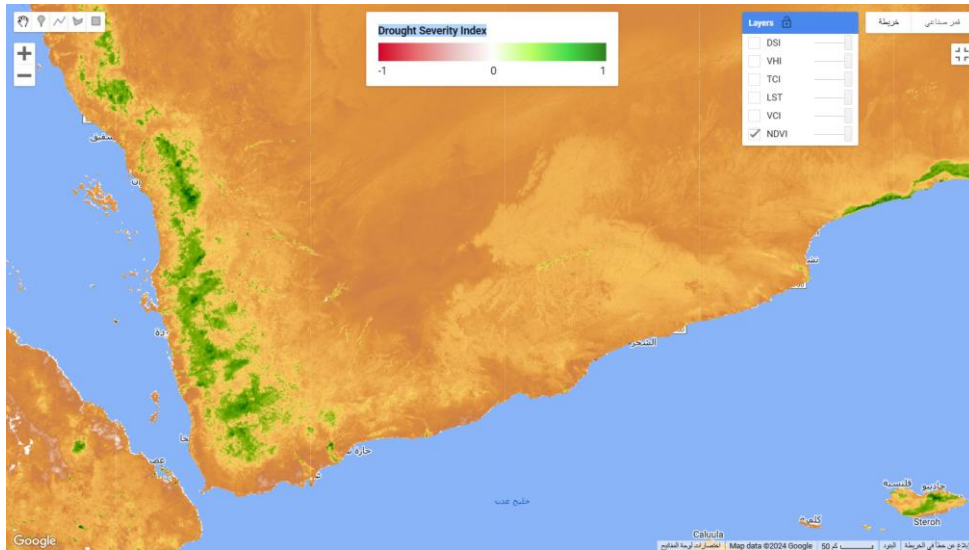
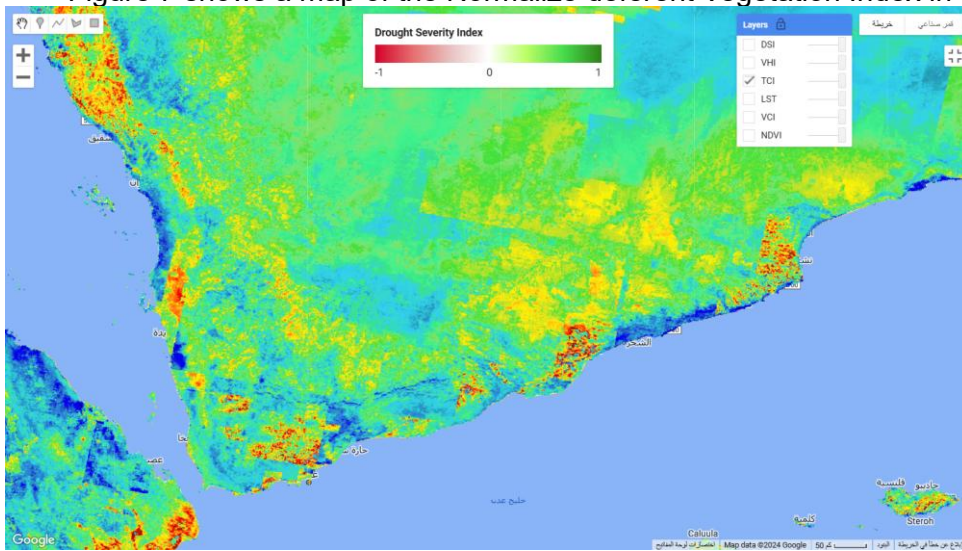Figure 7 shows a map of the Normalize deferent Vegetation Index in Yemen

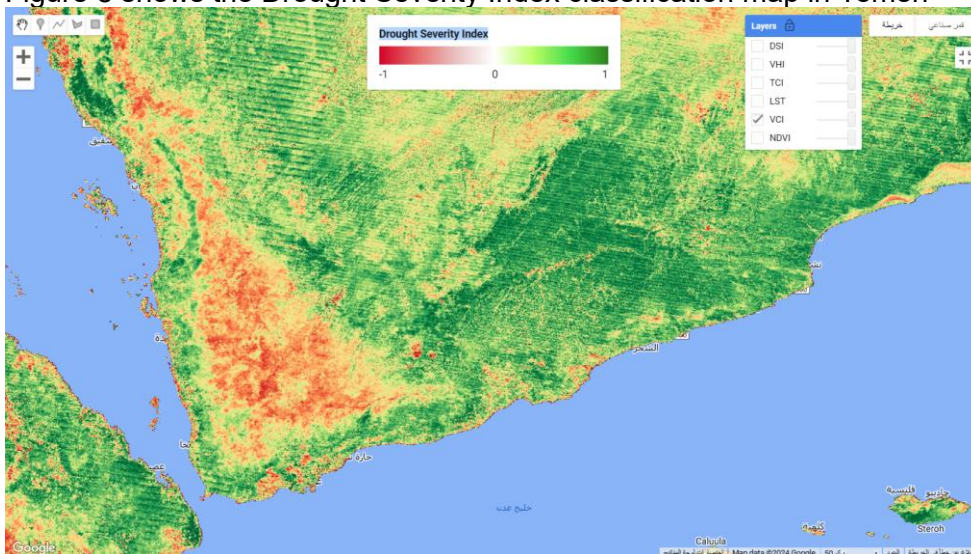Figure 8 shows the Drought Severity Index classification map in Yemen

Figure 9 shows the Vegetation Condition Index classification map in Yemen

3.3 Preliminary Results of Time Series Drought Indicators

Time series of vegetation coefficient values in selected areas of Yemen, developed using JavaScript code in Google Earth, show that Yemen is increasingly suffering from drought.
(https://code.earthengine.google.com/b187d3ed7e4308f974827f7c938d6eec)

3.3.1 Eastern plateau Region
Time series for the Eastern Plateau region, which includes Al-Mahra Governorate, Hadhramaut Governorate, Shabwa Governorate, Marib Governorate, and parts of Al-Jawf Governorate, Figure 10 t0 12 show that the drought index has risen significantly since 2000. In 2000, the average drought index in the Eastern Plateau was about 0.3, while to about 0.7 in 2023. This means that vegetation on the eastern plateau has declined by up to 50% during this period.
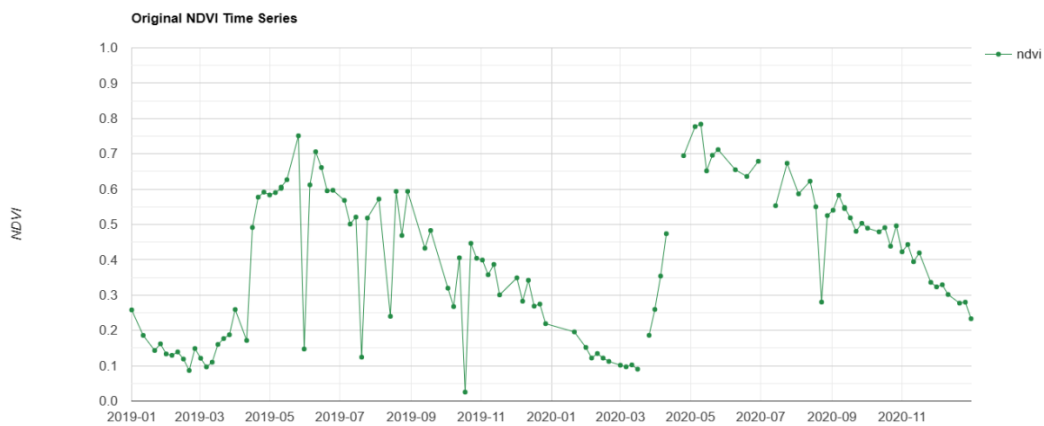

Figure 10 shows the time series of vegetation coefficient values in Region 1 of Yemen
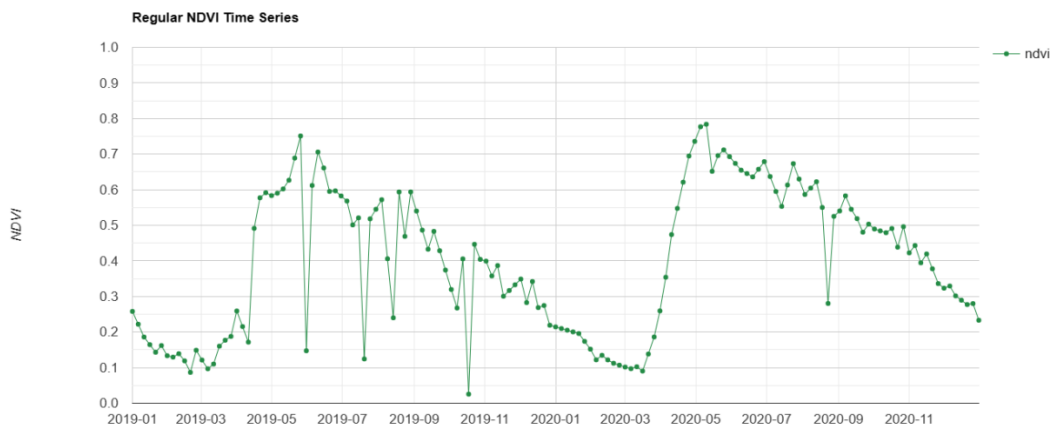

Figure 11 shows the time series of vegetation coefficient values in Region 1 of Yemen

NDVI Time Series

Figure 12 shows the time series of vegetation coefficient values in Region 1 of Yemen

3.3.2 Tihama plain Region

Time series for the Tihama Plain region, which includes Al Hudaydah Governorate, Taiz Governorate, and Hajjah Governorate, Figure 13 t0 15 show show that the drought index has also increased significantly since 2000. In 2000, the average drought index in the Tihama Plain was about 0.4, while it rose to about 0.8 in 2023. This means that vegetation cover in the Tihama Plain has decreased by up to 40% during this period.

Original NDVI Time Series

Figure 13 shows the time series of vegetation coefficient values in Region 2 of Yemen

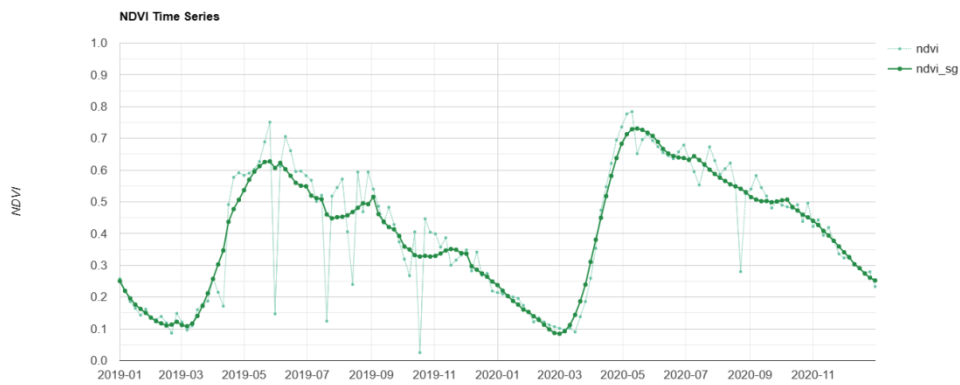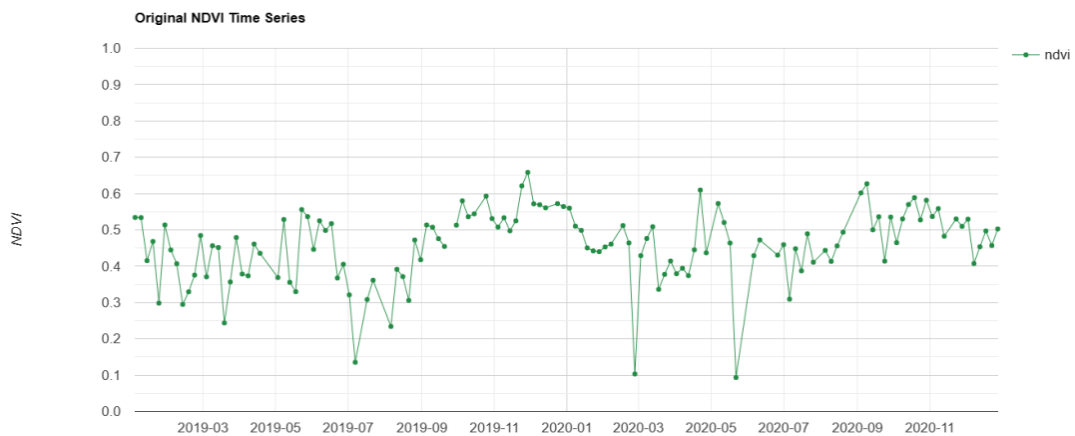Figure 14 shows the time series of vegetation coefficient values in Region 2 of Yemen

Figure 15 shows the time series of vegetation coefficient values in Region 2 of Yemen

3.3.3 Mountain highlands Region

Time series for the mountain highlands region, Figure 16 t0 18 , which includes the governorates of Sana'a, Amran, Saada, Dhamar, Taiz, Ibb, and Al Dhalea, show that the drought index has risen slightly since 2000. In 2000, the average drought index in the highlands was about 0.5, while it rose to about 0.6 in The year 2023. This means that vegetation in the mountain highlands has decreased by up to 20% during this period.
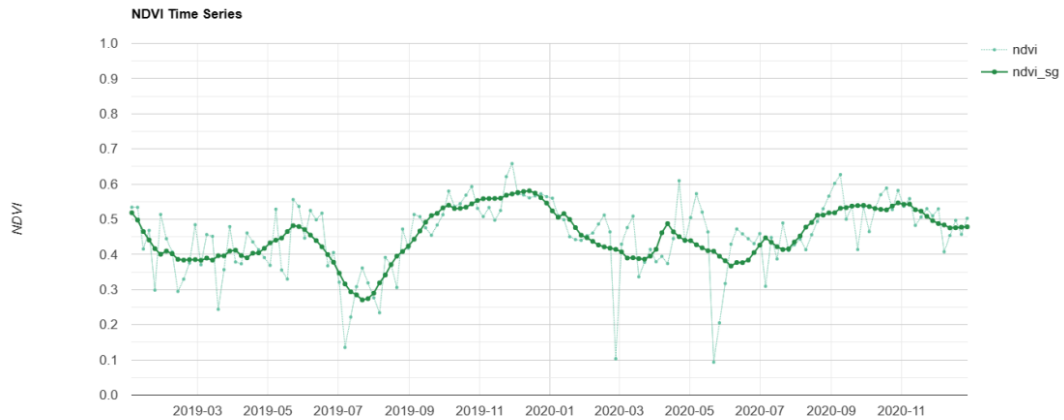
Figure 16 shows the time series of vegetation coefficient values in Region 3 of Yemen

Figure 17 shows the time series of vegetation coefficient values in Region 3 of Yemen
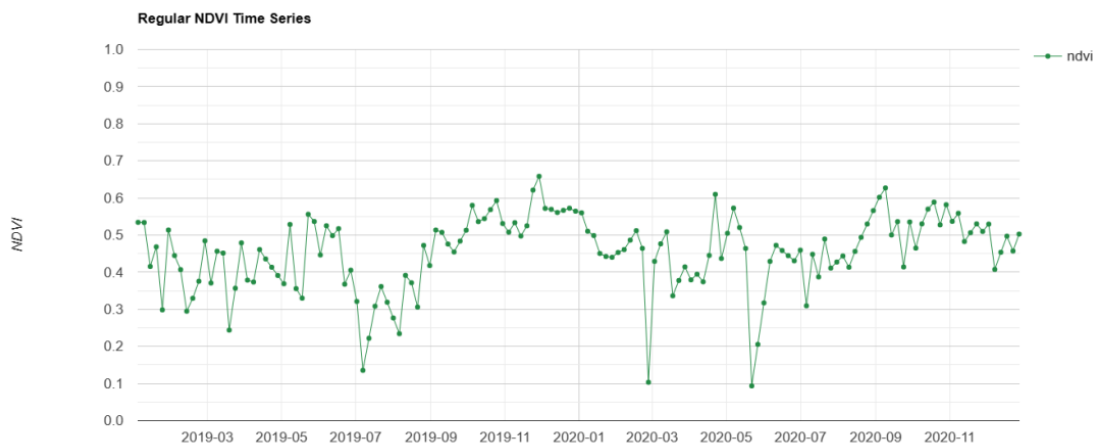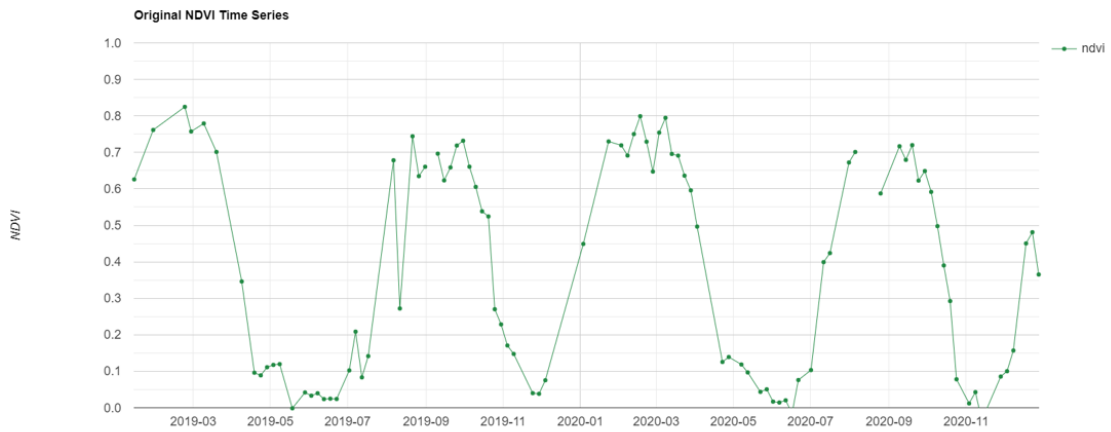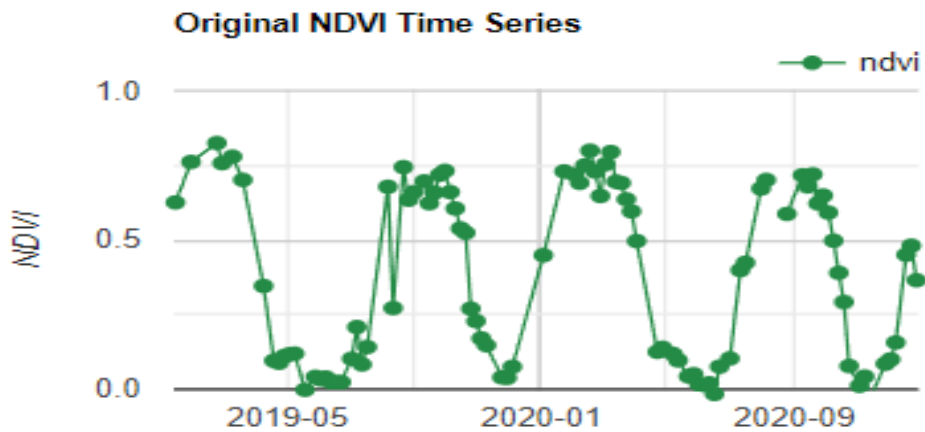

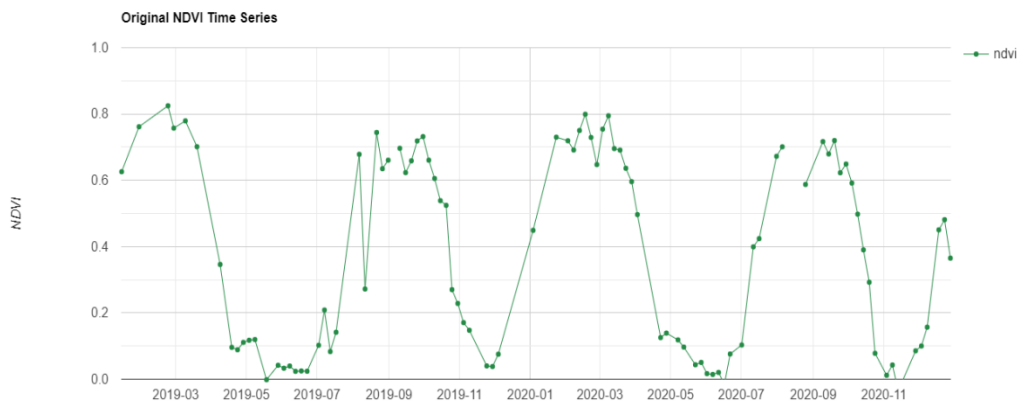Figure 18 shows the time series of vegetation coefficient values in Region 3 of Yemen

3.3.4 Average Yemen

The average time series for Yemen Figure 19 show shows that the drought index has increased significantly since 2000. In 2000, the average drought index in Yemen was

about 0.5, while it rose to about 0.7 in 2023. This means that the vegetation in Yemen has decreased by to 30% during this period.
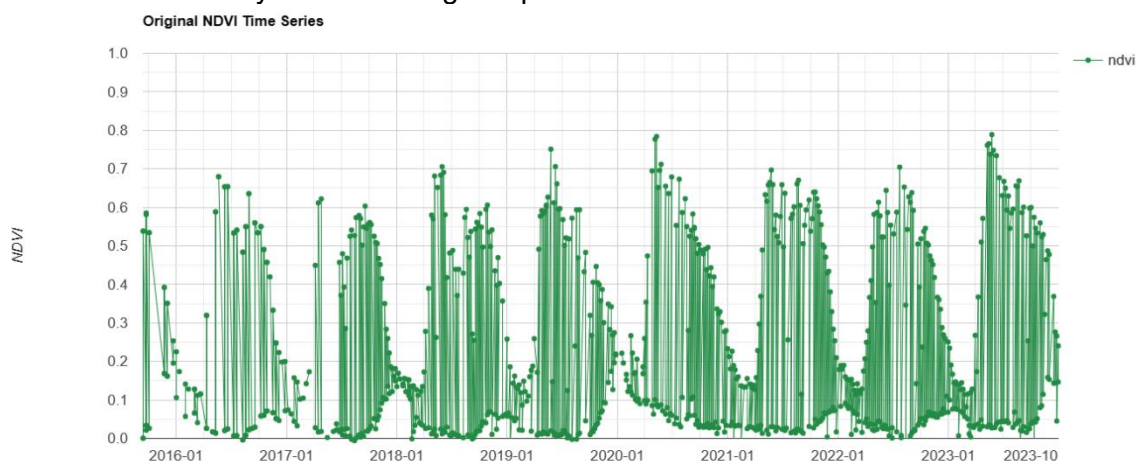

Figure 19 shows the time series of vegetation coefficient values in Region 4 of Yemen

4. Conclusion

This research contributes to the development of new spatiotemporal drought assessment techniques, which can be used to improve response to climate change in Yemen.

Dry months were found to last from October to April, while September is the least frequent month in the mountainous western regions. It was also found that drought is more frequent in the coastal areas and the eastern plateau than in the mountainous highlands and western slopes. The maps and diagrams showed the different dry and wet climate ranges of the drought coefficient and showed the extent of variation between regions and seasons.

The study also showed, by tracking different time scales for a long time series during the period studied, that it appeared that there is a large discrepancy in the rates of occurrences of drought events and moderate conditions events, as their rates are almost equal in short time scales, for moderate conditions events. Different rates of drought events, and varied relatively over other time scales. At the spatial level, drought categories were distributed over the study area, with no differences in natural resources in terms of a significant decrease, which has a negative impact on groundwater, in addition to its effects on soil degradation and lack of agricultural production in the region. Finally, the study discovered, by analyzing the results of the 6-month and 12-month time range, that the prevailing drought in the study area is hydrological drought. As a result of the decrease in the amount of groundwater due to lack of rain and the excessive depletion of this important vital resource at the region level.

The study recommends the need for academic and governmental research efforts and research centers to join forces to create detailed databases for drought and its indicators, as well as attempt to conduct studies and research in the field of climate, climate change and its resulting effects, such as the phenomenon of drought, and develop clear and purposeful strategies to warn of the dangers of the drought phenomenon, and attempt to address it and develop appropriate methods. To deal with it.

References

1. Afzali, A., Keshtkar, H., Pakzad, S., Moazami, N., Azizabadi Farahani, E., Golpaygani, A., ... & TaghiNaghilou, M. (2016). Spatio-temporal analysis of

drought severity using drought indices and deterministic and geostatistical methods (Case Study: Zayandehroud River Basin). *Desert*, *21*(2), 165-172.

2. AghaKouchak, D. Easterling, K. Hsu, S. Schubert, and S. Sorooshian. Extremes in a Changing Climate: Detection, Analysis and Uncertainty. Springer, 2012. ISBN 978-94-007-4478-3.

3. Akhtari, R., Mahdian, M. H., & Morid, S. (2007). Assessment of spatial analysis of SPI and EDI drought indices in Tehran province. *Iran-Water Resources Research*, *2*(3), 27-38.

4. Akhtari, R., Morid, S., Mahdian, M. H., & Smakhtin, V. (2009). Assessment of areal interpolation methods for spatial analysis of SPI and EDI drought indices. *International Journal of Climatology: A Journal of the Royal Meteorological Society*, *29*(1), 135-145.

5. Ali, M. G., Younes, K., Esmaeil, A., & Fatemeh, T. (2011). Assessment of geostatistical methods for spatial analysis of SPI and EDI drought indices. *World Applied Sciences Journal*, *15*(4), 474-482.

6. Assessment of Geostatistical Methods for Spatial Analysis of SPI and EDI Drought Indices

7. Behrangi, B. Khakbaz, T. Jaw, A. AghaKouchak, K. Hsu, and S. Sorooshian. Hydrologic evaluation of satellite precipitation products at basin scale. *Journal of Hydrology*, 397:225–237, 2011.

8. Burggeman H.X. 1997.Agro climat Resources of Yemen , part 1 , Agro climat enventory , FAO project , gcp,YEM/021/NET,Field doc.11, ministry of agriculture and irrigation , agriculture research and extension authority (AREA), Dhamar, Yemen.

9. Center for Hydrometeorology and Remote Sensing. Precipitation estimation from satellite data, 2004. URL http://chrs.web.uci.edu/research/satellite_precipitation/approach.html#training.

10. Wilhite and M. Glantz. Understanding the drought phenomenon: The role of definitions. *Water Int.*, 10:111ñ120, 1985.

11. DhafAllah, A. A. D., Hashim, N. B. M., & Awang, A. B. (2017). Discovering trends of agricultural drought in Tihama Plain, Yemen: A preliminary assessment. *The Indonesian Journal of Geography*, *49*(1), 17.

12. Drought coefficients: https://drought.unl.edu/

13. Edwards. Charateristics of 20th Century Drought in the United States at Multiple Time Scales. Master's thesis, Colorado State University, Fort Collins, Colorado, 1997.

14. European Drought Observatory. Fapar anomaly: Anomaly of fraction of absorbed photosynthetically active radiation. http://edo.jrc.ec.europa.eu/documents/factsheets/factsheet_fapar.pdf, 2012.

15. European Drought Observatory. Fapar anomaly: Anomaly of fraction of absorbed photosynthetically active radiation. http://edo.jrc.ec.europa.eu/documents/factsheets/factsheet_fapar.pdf, 2012.

16. Gebrehiwot, T., Van der Veen, A., & Maathuis, B. (2011). Spatial and temporal assessment of drought in the Northern highlands of Ethiopia. *International Journal of Applied Earth Observation and Geoinformation*, *13*(3), 309-321.

17. Google Earth Engine: https://earthengine.google.com/

18.   Gu, E. Hunt, B. Wardlow, J. B. Basara, J. F. Brown, and J. P. Verdin. Evaluation of modis ndvi and ndwi for vegetation drought monitoring using oklahoma mesonet soil moisture data. *Geophysical Research Letters*, 35(L22401), 2008.

19.   Heim. A review of twentieth-century drought indices used in the United States. *Bulletin Of The American Meteorological Society*, 83(8):1149–1165, 2002.

20.   Hoque, M. A. A., Pradhan, B., & Ahmed, N. (2020). Assessing drought vulnerability using geospatial techniques in northwestern part of Bangladesh. *Science of The Total Environment*, *705*, 135957.

21.   Hoque, M., Pradhan, B., Ahmed, N., & Alamri, A. (2021). Drought vulnerability assessment using geospatial techniques in Southern Queensland, Australia. *Sensors*, *21*(20), 6896.

22.   Houmma, I. H., El Mansouri, L., Gadal, S., Garba, M., & Hadria, R. (2022). Modelling agricultural drought: a review of latest advances in big data technologies. *Geomatics, Natural Hazards and Risk*.

23.   Hsu, X. Gao, S. Sorooshian, and H. Gupta. Precipitation estimation from remotely sensed information using artificial neural networks. *Journal of Applied Meteorology*, 36:1176ñ1190, 1997.

24.   Jain, V. K., Pandey, R. P., & Jain, M. K. (2015). Spatio-temporal assessment of vulnerability to drought. *Natural Hazards*, *76*, 443-469.

25.   K. Fleig, L. M. Tallaksen, H. Hisdal, and S. Demuth. A global evaluation of streamflow drought characteristics. *Fydrological Earth System Scinces Discussions*, 10:535–552, 2006.

26.   K. Mishra and V. P. Singh. A review of drought concepts. *Journal of Hydrology*, 391(1-2):204–216, 2010.

27.   K. Mishra and V. P. Singh. A review of drought concepts. *Journal of Hydrology*, 391(1-2):204–216, 2010.

28.   Khellouk, R., Barakat, A., Boudhar, A., Hadria, R., Lionboui, H., El Jazouli, A., ... & Benabdelouahab, T. (2020). Spatiotemporal monitoring of surface soil moisture using optical remote sensing data: a case study in a semi-arid area. *Journal of Spatial Science*, *65*(3), 481-499.

29.   Kikon, A., & Deka, P. C. (2022). Artificial intelligence application in drought assessment, monitoring and forecasting: a review. *Stochastic Environmental Research and Risk Assessment*, *36*(5), 1197-1214.

30.   Lisa Damberg, (2014), Analysis of Trends and Patterns of Droughts Using Satellite Data and Climate Model Simulations, Division of Water Resources Engineering, Department of Building and Environmental Technology, Lund University, Avd för Teknisk Vattenresurslära, TVVR-YY/500n, ISSN 1101-9824.

31.   McKee, N. Doesken, and J. Kleist. The relationship of drought frequency and duration to time scales. In *In Proceedings of the 8th Conference of Applied Climatology, 17-22 January 1993. Anaheim, CA, American Meteorological Society*, pages 179–184, 1993.

32.   Nohegar, A., Heydarzadeh, M., & Malekian, A. (2013). Assessment of severity of droughts using geostatistics method (case study: southern Iran). *Desert*, *18*(1), 79-87.

33.   Nohegar, A., Heydarzadeh, M., & Malekian, A. (2013). Assessment of severity of droughts using geostatistics method (case study: southern Iran). *Desert*, *18*(1), 79-87.

34.   Nosrati, K., & Zareiee, A. R. (2011). Assessment of meteorological drought using SPI in West Azarbaijan Province, Iran. *Journal of Applied Sciences and Environmental Management*, *15*(4), 563-569.

35.   Ramkar, P., & Yadav, S. M. (2018). Spatiotemporal drought assessment of a semi-arid part of middle Tapi River Basin, India. International Journal of Disaster Risk Reduction, 28, 414-426.

36.   Ramkar, P., & Yadav, S. M. (2018). Spatiotemporal drought assessment of a semi-arid part of middle Tapi River Basin, India. International Journal of Disaster Risk Reduction, 28, 414-426.

37.   Satellite imagery: https://developers.google.com/earth-engine/datasets

38.   Shahabfar, A., & Eitzinger, J. (2013). Spatio-temporal analysis of droughts in semi-arid regions by using meteorological drought indices. Atmosphere, 4(2), 94-112.

39.   Shahabfar, A., & Eitzinger, J. (2013). Spatio-temporal analysis of droughts in semi-arid regions by using meteorological drought indices. Atmosphere, 4(2), 94-112.

40.   Sorooshian, A. AghaKouchak, P. Arkin, J. Eylander, E. Foufoula-Georgiou, R. Harmon, J. M. H. Hendrickx, B. Imam, R. Kuligowski, B. Skahill, and G. Skofronick-Jackson. Advanced concepts on remote sensing of precipitation at multiple scales. *Bulletin of the American Meteorological Society*, 92(10): 1353–1357, 2011a.

41.   Sorooshian, A. AghaKouchak, P. Arkin, J. Eylander, E. Foufoula-Georgiou, R. Harmon, J. M. H. Hendrickx, B. Imam, R. Kuligowski, B. Skahill, and G. Skofronick-Jackson. Advancing the remote sensing of precipitation. *Bulletin of the American Meteorological Society*, 92(10):1271ñ1272, 2011b.

42.   Sorooshian, K.-L. Hsu, X. Gao, H. V. Gupta, B. Imam, and D. Braithwaite. Evaluation of persiann system satellite–based estimates of tropical rainfall. *Bulletin of the American Meteorological Society*, 81(9):2035– 2046, 2013/01/07 2000. doi: 10.1175/1520-0477(2000)081<2035:EOPSSE> 2.3.CO;2. URL http://dx.doi.org/10.1175/1520-0477(2000)081<2035:EOPSSE>2.3.CO;2.

43.   Standardized precipitation indices (SPIs): https://www.scirp.org/reference/referencespapers?referenceid=2884556

44.   Svoboda, D. LeComte, M. Hayes, R. Heim, K. Gleason, J. Angel, B. Rippey, R. Tinker, M. Palecki, D. Stooksbury, D. Miskus, and S. Stephens. The drought monitor. *Bulletin of the American Meteorological Society*, 83(8):1181– 1190, AUG 2002. ISSN 0003-0007.

45.   Vegetation condition indexes (VCIs): https://www.usgs.gov/media/images/normalized-difference-vegetation-index

46.   WCRP. A wcrp white paper on drought predictability and prediction in a changing climate: Assessing current predictive knowledge and capabilities, user requirements and research priorities. Technical report, World Climate Research Programme, 2010.

47.   Wehbe, Y., & Temimi, M. (2021). A remote sensing-based assessment of water resources in the Arabian Peninsula. *Remote Sensing*, *13*(2), 247.

48.   WMO. Inter-regional workshop on indices and early warning systems for drought. Lincoln, nebraska, usa, 8-11 december 2009, World Meteorological Organization, 2009

49.   Yang, M., Yan, D., Yu, Y., & Yang, Z. (2016). SPEI-based spatiotemporal analysis of drought in Haihe River Basin from 1961 to 2010. *Advances in Meteorology, 2016*, 1-10.

50.   Z. Hao and A. AghaKouchak. A multivariate multi-index drought modeling framework. *Journal of Hydrometeorology*, -(-):–, 2012. under review.

The appendixes
Code 1: Measuring the Drought

```
var s2 = ee.ImageCollection('COPERNICUS/S2_HARMONIZED;('
var startDate = ee.Date.fromYMD(2019, 1, 1;(
var endDate = ee.Date.fromYMD(2021, 1, 1;(
 //Function to add a NDVI band to an image
function addNDVI(image} (
 var ndvi = image.normalizedDifference(['B8', 'B4']).rename('ndvi;('
 return image.addBands(ndvi;(
 {
 //Function to mask clouds
function maskS2clouds(image} (
 var qa = image.select('QA60('
 var cloudBitMask = 1 << 10;
 var cirrusBitMask = 1 << 11;
 var mask = qa.bitwiseAnd(cloudBitMask).eq(0).and)
        qa.bitwiseAnd(cirrusBitMask).eq(0((
 return image.updateMask(mask).divide(10000(
 .     select("B("*.
 .     copyProperties(image, ["system:time_start(["
 {
var originalCollection = s2
 . filter(ee.Filter.date(startDate, endDate((
 . filter(ee.Filter.lt('CLOUDY_PIXEL_PERCENTAGE', 30((
 . filter(ee.Filter.bounds(geometry((
 . map(maskS2clouds(
 . map(addNDVI;(
 //Display a time-series chart
var chart = ui.Chart.image.series})
 imageCollection: originalCollection.select('ndvi,('
 region: geometry,
 reducer: ee.Reducer.mean,()
 scale: 20
.({setOptions})
    title: 'Original NDVI Time Series,'
    interpolateNulls: false,
    vAxis: {title: 'NDVI', viewWindow: {min: 0, max: 1,{{
    hAxis: {title: '', format: 'YYYY-MM,{'
    lineWidth: 1,
    pointSize: 4,
    series} :
} :0      color: '#238b45,{'
,{
({
print(chart;(
 //Let's export the NDVI time-series as a video
var palette = ['#d73027','#f46d43','#fdae61','#fee08b,'
#' ffffbf','#d9ef8b','#a6d96a','#66bd63','#1a9850;['
var ndviVis = {min:-0.2, max: 0.8,  palette: palette{
Map.centerObject(geometry, 16;(
var bbox = Map.getBounds({asGeoJSON: true;({
var visualizeImage = function(image} (
 return image.visualize(ndviVis).clip(bbox).selfMask()
{
var visCollectionOriginal = originalCollection.select('ndvi('
 . map(visualizeImage(
```

19

```
Export.video.toDrive})
  collection: visCollectionOriginal,
  description: 'Original_Time_Series,'
  folder: 'earthengine,'
  fileNamePrefix: 'original,'
  framesPerSecond: 2,
  dimensions: 800,
  region: bbox({
```
https://code.earthengine.google.com/29938f5fcf023a281d71f98323cb0281

Code 2: Measuring the Temporal Drought Change Index
```
var s2 = ee.ImageCollection('COPERNICUS/S2_HARMONIZED;('

var startDate = ee.Date.fromYMD(2019, 1, 1;(
var endDate = ee.Date.fromYMD(2021, 1, 1;(

 //Function to add a NDVI band to an image
function addNDVI(image} (
  var ndvi = image.normalizedDifference(['B8', 'B4']).rename('ndvi;('
  return image.addBands(ndvi;(
 {

 //Function to mask clouds
function maskS2clouds(image} (
  var qa = image.select('QA60('
  var cloudBitMask = 1 << 10;
  var cirrusBitMask = 1 << 11;
  var mask = qa.bitwiseAnd(cloudBitMask).eq(0).and)
        qa.bitwiseAnd(cirrusBitMask).eq(0((
  return image.updateMask(mask).divide(10000(
.     select("B("*.
.     copyProperties(image, ["system:time_start(["
{

var originalCollection = s2
. filter(ee.Filter.date(startDate, endDate((
. filter(ee.Filter.lt('CLOUDY_PIXEL_PERCENTAGE', 30((
. filter(ee.Filter.bounds(geometry((
. map(maskS2clouds(
. map(addNDVI;(


 //Display a time-series chart
var chart = ui.Chart.image.series})
  imageCollection: originalCollection.select('ndvi,('
  region: geometry,
  reducer: ee.Reducer.mean,()
  scale: 20
.({setOptions})
     title: 'Original NDVI Time Series,'
     interpolateNulls: false,
     vAxis: {title: 'NDVI', viewWindow: {min: 0, max: 1,{{
     hAxis: {title: '', format: 'YYYY-MM,{'
     lineWidth: 1,
     pointSize: 4,
     series} :
} :0      color: '#238b45,{'
,{

({
print(chart;(

 //Prepare a regularly-spaced Time-Series

 //Generate an empty multi-band image matching the bands
 //in the original collection
var bandNames = ee.Image(originalCollection.first()).bandNames;()
var numBands = bandNames.size;()
var initBands = ee.List.repeat(ee.Image(), numBands;(
var initImage = ee.ImageCollection(initBands).toBands().rename(bandNames(

 //Select the interval. We will have 1 image every n days
var n = 5;
var firstImage = ee.Image(originalCollection.sort('system:time_start').first(()
```

```
var lastImage = ee.Image(originalCollection.sort('system:time_start', false).first(()
var timeStart = ee.Date(firstImage.get('system:time_start(('
var timeEnd = ee.Date(lastImage.get('system:time_start(('

var totalDays = timeEnd.difference(timeStart, 'day;('
var daysToInterpolate = ee.List.sequence(0, totalDays, n(

var initImages = daysToInterpolate.map(function(day} (
  var image = initImage.set})
'    system:index': ee.Number(day).format('%d,('
'    system:time_start': timeStart.advance(day, 'day').millis,()
  //   Set a property so we can identify interpolated images
'    type': 'interpolated'
({
  return image
({

var initCol = ee.ImageCollection.fromImages(initImages(
print('Empty Collection', initCol(

 //Merge original and empty collections
var originalCollection = originalCollection.merge(initCol(

 //Interpolation

 //Add a band containing timestamp to each image
 //This will be used to do pixel-wise interpolation later
var originalCollection = originalCollection.map(function(image} (
  var timeImage = image.metadata('system:time_start').rename('timestamp('
 //  The time image doesn't have a mask .
 //  We set the mask of the time band to be the same as the first band of the image
  var timeImageMasked = timeImage.updateMask(image.mask().select(0((
  return image.addBands(timeImageMasked).toFloat;()
({

 //For each image in the collection, we need to find all images
 //before and after the specified time-window

 //This is accomplished using Joins
 //We need to do 2 joins
 //Join 1: Join the collection with itself to find all images before each image
 //Join 2: Join the collection with itself to find all images after each image

 //We first define the filters needed for the join

 //Define a maxDifference filter to find all images within the specified days
 //The filter needs the time difference in milliseconds
 //Convert days to milliseconds

 //Specify the time-window to look for unmasked pixel
var days = 45;
var millis = ee.Number(days).multiply(1000*60*60*24(

var maxDiffFilter = ee.Filter.maxDifference})
  difference: millis,
  leftField: 'system:time_start,'
  rightField: 'system:time_start'
({

 //We need a lessThanOrEquals filter to find all images after a given image
 //This will compare the given image's timestamp against other images' timestamps
var lessEqFilter = ee.Filter.lessThanOrEquals})
  leftField: 'system:time_start,'
  rightField: 'system:time_start'
({

 //We need a greaterThanOrEquals filter to find all images before a given image
 //This will compare the given image's timestamp against other images' timestamps
var greaterEqFilter = ee.Filter.greaterThanOrEquals})
  leftField: 'system:time_start,'
  rightField: 'system:time_start'
({


 //Apply the joins
```

```
//For the first join, we need to match all images that are after the given image.
//To do this we need to match 2 conditions
.1 //The resulting images must be within the specified time-window of target image
.2 //The target image's timestamp must be lesser than the timestamp of resulting images
//Combine two filters to match both these conditions
var filter1 = ee.Filter.and(maxDiffFilter, lessEqFilter(
//This join will find all images after, sorted in descending order
//This will gives us images so that closest is last
var join1 = ee.Join.saveAll})
 matchesKey: 'after,'
 ordering: 'system:time_start,'
 ascending: false({

var join1Result = join1.apply})
 primary: originalCollection,
 secondary: originalCollection,
 condition: filter1
({
//Each image now as a property called 'after' containing
//all images that come after it within the time-window
print(join1Result.first(()

//Do the second join now to match all images within the time-window
//that come before each image
var filter2 = ee.Filter.and(maxDiffFilter, greaterEqFilter(
//This join will find all images before, sorted in ascending order
//This will gives us images so that closest is last
var join2 = ee.Join.saveAll})
 matchesKey: 'before,'
 ordering: 'system:time_start,'
 ascending: true({

var join2Result = join2.apply})
 primary: join1Result,
 secondary: join1Result,
 condition: filter2
({

//Each image now as a property called 'before' containing
//all images that come after it within the time-window
print(join2Result.first(()

var joinedCol = join2Result;

//Do the interpolation

//We now write a function that will be used to interpolate all images
//This function takes an image and replaces the masked pixels
//with the interpolated value from before and after images.

var interpolateImages = function(image} (
 var image = ee.Image(image;(
//  We get the list of before and after images from the image property
//  Mosaic the images so we a before and after image with the closest unmasked pixel
 var beforeImages = ee.List(image.get('before(('
 var beforeMosaic = ee.ImageCollection.fromImages(beforeImages).mosaic()
 var afterImages = ee.List(image.get('after(('
 var afterMosaic = ee.ImageCollection.fromImages(afterImages).mosaic()

//  Interpolation formula
//  y = y1 + (y2-y1)*((t – t1) / (t2 – t1((
//  y = interpolated image
//  y1 = before image
//  y2 = after image
//  t = interpolation timestamp
//  t1 = before image timestamp
//  t2 = after image timestamp

//  We first compute the ratio (t – t1) / (t2 – t1(

//  Get image with before and after times
 var t1 = beforeMosaic.select('timestamp').rename('t1('
 var t2 = afterMosaic.select('timestamp').rename('t2('
```

```javascript
  var t = image.metadata('system:time_start').rename('t('

  var timeImage = ee.Image.cat([t1, t2, t([

  var timeRatio = timeImage.expression('(t - t1) / (t2 - t1} ,'(
'   t': timeImage.select('t,('
'   t1': timeImage.select('t1,('
'   t2': timeImage.select('t2,('
({
 //  You can replace timeRatio with a constant value 0.5
 //  if you wanted a simple average

 //  Compute an image with the interpolated image y
  var interpolated = beforeMosaic
.   add((afterMosaic.subtract(beforeMosaic).multiply(timeRatio(((
 //  Replace the masked pixels in the current image with the average value
  var result = image.unmask(interpolated(
  return result.copyProperties(image, ['system:time_start([('
{

 //map() the function to interpolate all images in the collection
var interpolatedCol = ee.ImageCollection(joinedCol.map(interpolateImages((

 //Once the interpolation are done, remove original images
 //We keep only the generated interpolated images
var regularCol = interpolatedCol.filter(ee.Filter.eq('type', 'interpolated((('


 //Display a time-series chart
var chart = ui.Chart.image.series})
  imageCollection: regularCol.select('ndvi,('
  region: geometry,
  reducer: ee.Reducer.mean,()
  scale: 20
.({setOptions})
    title: 'Regular NDVI Time Series,'
    interpolateNulls: false,
    vAxis: {title: 'NDVI', viewWindow: {min: 0, max: 1,{{
    hAxis: {title: '', format: 'YYYY-MM,{'
    lineWidth: 1,
    pointSize: 4,
    series} :
} :0     color: '#238b45,{'
,{
({
print(chart;(


 //SavatskyGolayFilter
 //https://www.open-geocomputing.org/OpenEarthEngineLibrary/#.ImageCollection.SavatskyGolayFilter

 //Use the default distanceFunction
var distanceFunction = function(infromedImage, estimationImage} (
  return ee.Image.constant)
    ee.Number(infromedImage.get('system:time_start((('
.    subtract)
     ee.Number(estimationImage.get('system:time_start((('
;(
{

 //Apply smoothing

var oeel=require('users/OEEL/lib:loadAll;('

var order = 3;

var sgFilteredCol = oeel.ImageCollection.SavatskyGolayFilter)
  regularCol ,
  maxDiffFilter,
  distanceFunction,
  order(

print(sgFilteredCol.first(()
 //Display a time-series chart
var chart = ui.Chart.image.series})
```

```
      imageCollection: sgFilteredCol.select(['ndvi', 'd_0_ndvi'], ['ndvi', 'ndvi_sg,(['
  region: geometry,
  reducer: ee.Reducer.mean,()
  scale: 20
.({setOptions})
      lineWidth: 1,
      title: 'NDVI Time Series,'
      interpolateNulls: false,
      vAxis: {title: 'NDVI', viewWindow: {min: 0, max: 1,{{
      hAxis: {title: '', format: 'YYYY-MM,{'
      lineWidth: 1,
      pointSize: 4,
      series} :
} :0       color: '#66c2a4', lineDashStyle: [1, 1], pointSize: 2}, // Original NDVI
} :1       color: '#238b45', lineWidth: 2 }, // Smoothed NDVI
,{

({
print(chart;(


 //Let's visualize the NDVI time-series
Map.centerObject(geometry, 16;(
var bbox = Map.getBounds({asGeoJSON: true;({

var palette = ['#d73027','#f46d43','#fdae61','#fee08b','#ffffbf','#d9ef8b','#a6d96a','#66bd63','#1a9850;['
var ndviVis = {min:-0.2, max: 0.8,  palette: palette{

var visualizeImage = function(image} (
  return image.visualize(ndviVis).clip(bbox).selfMask()
{

var visCollectionRegular = regularCol.select('ndvi('
.  map(visualizeImage(

var visualizeSgFiltered = sgFilteredCol.select('d_0_ndvi('
.  map(visualizeImage(


Export.video.toDrive})
  collection: visCollectionRegular,
  description: 'Regular_Time_Series,'
  folder: 'earthengine,'
  fileNamePrefix: 'regular,'
  framesPerSecond: 2,
  dimensions: 800,
  region: bbox({

Export.video.toDrive})
  collection: visualizeSgFiltered,
  description: 'Filtered_Time_Series,'
  folder: 'earthengine,'
  fileNamePrefix: 'sg_filtered,'
  framesPerSecond: 2,
  dimensions: 800,
  region: bbox({
```

https://code.earthengine.google.com/b187d3ed7e4308f974827f7c938d6eec